

**Motion of a current-vortex sheet in the magnetic Kelvin-Helmholtz instability**

Seunghyeon Baek

*Department of Applied Mathematical Sciences, Korea University, Sejong 30019, South Korea*Sung-Ik Sohn \**Department of Mathematics, Gangneung-Wonju National University, Gangneung 25457, South Korea*

(Received 13 March 2023; accepted 30 August 2023; published 19 September 2023)

In this paper, we consider the Kelvin-Helmholtz instability in the magnetohydrodynamic flow. The motion of the interface is described by a current-vortex sheet. We examine the linear stability of the current-vortex sheet model and determine the growth rate of the interface. The interface is linearly stable for  $M_A < 2$  where  $M_A$  represents the Alfvén Mach number. It is found that the interface is linearly unstable in the limit of the critical Alfvén Mach number  $M_A = 2$ , due to resonance of eigenvalues. We perform numerical simulations for the current-vortex sheet for both regimes of  $M_A < 2$  and  $M_A > 2$ . The numerical results show the stabilizing effects of the magnetic field on the evolution of the current-vortex sheet when the magnetic field is sufficiently large. For the regime  $M_A < 2$ , the sheet oscillates both longitudinally and transversely and the transverse surface wave is pronounced for a large  $M_A$ . Remarkably, the interface is nonlinearly unstable for  $M_A \approx 2$ , for  $M_A < 2$ , which may be due to the propagation of surface waves. For the regime  $M_A > 2$ , the roll-up of the spiral is weakened and the spiral is more pinched and stretched for smaller  $M_A$ . A comparison of the unstable evolutions of large and small values of  $M_A$  shows significant differences of the magnetic field and vortex sheet strength.

DOI: [10.1103/PhysRevE.108.035107](https://doi.org/10.1103/PhysRevE.108.035107)**I. INTRODUCTION**

The Kelvin-Helmholtz instability (KHI) is a basic physical process and arises in a velocity shear flow. Strong roll-ups usually evolve on the interface and result in a small-scale structure and eventually turbulent mixing of the fluid [1–3]. The KHI is widely found in natural or astrophysical environments, such as billowing clouds, internal stratified ocean [4], astrophysical jets [5], solar wind-magnetopause interaction [6,7], and supernova explosions [8]. While the phenomenon is well understood in fluid dynamics, it is much more challenging in magnetohydrodynamic (MHD) flows.

The KHI in magnetic fields has been studied extensively. Theoretical studies of the KHI in MHD flows started from the linear stability analysis by Chandrasekhar [9], for incompressible inviscid cases. Miura and Pritchett [10] extended the linear analysis to compressible MHD flows. The stability of steady MHD flows with current-vortex sheets was investigated by Ilin *et al.* [11]. Hunter and Thoo [12] presented a weakly nonlinear analysis for the MHD KHI and discussed the ill-posedness of the solution from the propagation of nonlinear surface waves.

The nonlinear evolution of the MHD KHI has been studied through numerical simulations. Malagoli *et al.* [13] examined the effects of the Mach number, the ratio of the Alfvén speed to the sound speed, and the effective diffusivity upon the evolution and saturation of the KHI. Dahlbug *et al.* [14] reported that the character of the instability changes depending on the width of the current-vortex sheet. The growth and saturation of the KHI with parallel and anti-parallel magnetic fields was considered by Keppens *et al.* [15]. They showed that the magnetic tension force can stabilize the instability and reduces the growth rate. The formation of surface waves in the KHI in a compressible plasma was discussed in Lai and Lyu [16]. More recently, Liu *et al.* [17] explored the physical effects of the transverse magnetic pressure and magnetic tension on the instability and showed that both have effects on the suppression process.

Despite the significance of vortex sheets in the MHD flows, a few theoretical models have been proposed to investigate the nonlinear motion of fluid instabilities. Matsuoka *et al.* [18,19] proposed a vortex sheet model to describe the Richtmyer-Meshkov instability, which is an interfacial instability driven by a shock wave, in a MHD flow. The density jump in the Richtmyer-Meshkov instability induces two different magnetic fields across the interface, and the tangential discontinuities of magnetic fields induce a nonuniform current-vortex sheet. They also applied the current-vortex sheet model to study the nonlinear evolution of the MHD KHI [20]. However, they considered only the regime of weak magnetic fields, where the nonlinear evolution of the interface does not significantly differ from that in the pure hydrodynamic flows [21,22]. Moreover, they presented the linear

\*sohnsi@gwnu.ac.kr

stability analysis for the Richtmyer-Meshkov instability and obtained the dispersion relation for standing waves, in the stable case. Their analysis is based essentially on the MHD equations, not directly using the integral equation of the vortex sheet model.

In this paper, we consider the current-vortex sheet model for a parallel magnetic field. We present the linear stability analysis from the current-vortex sheet model and determine the growth rate to identify linearly stable and unstable regimes of the MHD KHI. We also investigate the nonlinear evolution of the MHD KHI for a wide range of magnetic fields, for both unstable and stable regimes. For this purpose, we perform numerical simulations using the vortex blob method [21,23].

An important question is whether the KHI in the MHD flow is nonlinearly stable in the linearly stable regime. In the hydrodynamic flows, the interface in the linearly stable regime either does not grow or merely oscillates with an initial mode, when surface tension is strong enough, or the density ratio of upper and lower fluids is infinite in the absence of surface tension [24,25]. Therefore, the KHI in the hydrodynamic flows is always stable when it is linearly stable. However, there have been only a few literatures on the nonlinear stability of the MHD KHI, with a sharp velocity jump. In this paper, we will address the issue of the nonlinear stability of the MHD KHI.

In Sec. II, we describe the model of the current-vortex sheet. In Sec. III, we present the linear stability analysis of the model and find the growth rate. In Sec. IV, the numerical method is described briefly and numerical results for the evolution of the MHD KHI are presented for both linearly stable and unstable regimes. Section V gives conclusions.

## II. VORTEX SHEET MODEL IN MHD FLOWS

We consider an inviscid and incompressible MHD fluid in two-dimensions. The governing equations for the flow are given by

$$\frac{\partial \mathbf{u}}{\partial t} + \mathbf{u} \cdot \nabla \mathbf{u} - \frac{1}{\rho \mu} \mathbf{B} \cdot \nabla \mathbf{B} = -\frac{1}{\rho} \nabla \left( p + \frac{1}{2\mu} \mathbf{B} \cdot \mathbf{B} \right), \quad (1)$$

$$\frac{\partial \mathbf{B}}{\partial t} = \nabla \times (\mathbf{u} \times \mathbf{B}), \quad (2)$$

$$\nabla \cdot \mathbf{u} = 0, \quad (3)$$

$$\nabla \cdot \mathbf{B} = 0, \quad (4)$$

$$\mu \mathbf{j} = \nabla \times \mathbf{B}, \quad (5)$$

where  $\mathbf{u}$  denotes the fluid velocity,  $\rho$  the fluid density,  $\mu$  the permeability,  $\mathbf{B}$  the magnetic field, and  $p$  the fluid pressure.

We consider an interface with tangential velocity jump. The velocity jump induces two different magnetic fields  $\mathbf{B}_1$  and  $\mathbf{B}_2$  between the interface. From the tangential discontinuities of the fluid velocity and magnetic field, the interface becomes a current-vortex sheet. We assume that the interface is periodic in the  $x$  direction with period  $L = 2\pi$  and the free stream velocity is  $\mp U$  at  $y = \pm\infty$ . The interface can be described by a parametric curve  $\mathbf{x}(\theta, t) = (x(\theta, t), y(\theta, t))$  for  $0 \leq \theta \leq 2\pi$ .

The evolution of the interface is given by

$$\frac{d\mathbf{x}}{dt} = \mathbf{q}, \quad (6)$$

where  $\mathbf{q}$  is the interface velocity. By rewriting the location of the interface  $z = x + iy$  and the interface velocity  $q = u + iv$  in the complex form, the interface velocity is given by the Birkhoff-Rott equation [1]:

$$q^*(\theta, t) = \frac{1}{4\pi i} \text{P.V.} \int_0^{2\pi} \gamma(\theta', t) \cot \left( \frac{z(\theta, t) - z(\theta', t)}{2} \right) \times s_\theta(\theta') d\theta', \quad (7)$$

where P.V. represents the principal value integral and  $s$  is the arclength. The subscript  $\theta$  denotes the partial derivative with respect to it. The vortex sheet strength is defined as

$$\gamma(\theta, t) = \frac{\partial \Gamma}{\partial s}(\theta, t), \quad (8)$$

where  $\Gamma$  is the circulation at the sheet. The vortex sheet strength gives the tangential velocity difference across the interface by

$$\gamma(\theta, t) = (\mathbf{u}_1 - \mathbf{u}_2) \cdot \mathbf{t}, \quad (9)$$

where  $\mathbf{u}_1$  and  $\mathbf{u}_2$  are the velocities below and above the interface, and  $\mathbf{t}$  is the unit tangent vector to the interface.

From the continuity of the total pressure  $P = p + \mu \mathbf{B} \cdot \mathbf{B}/2$  at the interface and Eq. (1), the evolution equation for the circulation is obtained as

$$\frac{d\Gamma}{dt} = \frac{1}{\rho \mu} \langle \mathbf{B} \rangle \cdot \mathbf{j}_s, \quad (10)$$

where  $\langle \mathbf{B} \rangle = (\mathbf{B}_1 + \mathbf{B}_2)/2$ , and  $\mathbf{j}_s = \mathbf{B}_1 - \mathbf{B}_2$  denotes the surface current density. The current sheet strength is given by  $j_s = \mathbf{j}_s \cdot \mathbf{t}$ . Differentiating Eq. (10) with respect to  $s$ , we have the evolution equation for the vortex sheet strength,

$$\frac{d\gamma}{dt} = \frac{1}{\rho \mu s_\theta} \langle \langle \mathbf{B} \rangle \cdot \mathbf{j}_s \rangle_\theta. \quad (11)$$

It was shown for the normal component of the magnetic field [18,19] that

$$\frac{d}{dt} (\mathbf{B}_i \cdot \mathbf{n}) = 0, \quad \text{for } i = 1, 2, \quad (12)$$

if  $\mathbf{B}_i \cdot \mathbf{n} = 0$  is satisfied at  $t = 0$ , where  $\mathbf{n}$  is the unit normal vector to the interface. This equation means that the magnetic field does not have the normal component at the interface for  $t > 0$  if the magnetic field is applied parallel to the interface initially, i.e.,  $\mathbf{B}_i = B_i^t \mathbf{t}$ . We then consider only the tangential component of the magnetic field. From the induction equation [18,19], we have

$$\frac{dB_1^t}{dt} = -\frac{1}{2s_\theta} \gamma (B_1^t)_\theta + \frac{B_1^t}{s_\theta} \left( q_\theta^t + \frac{\gamma_\theta}{2} \right), \quad (13a)$$

$$\frac{dB_2^t}{dt} = \frac{1}{2s_\theta} \gamma (B_2^t)_\theta + \frac{B_2^t}{s_\theta} \left( q_\theta^t - \frac{\gamma_\theta}{2} \right), \quad (13b)$$

where  $q^t$  denotes the tangential component of the interface velocity  $\mathbf{q}$ . Equations (6), (7), (11), and (13) determine the motion of a current-vortex sheet when the magnetic field is applied parallel to the interface.

### III. LINEAR STABILITY ANALYSIS

In this section, we present the linear stability analysis of the current-vortex sheet model described in the previous section. The flat interface  $x(\theta, t) = \theta$ ,  $y(\theta, t) = 0$  with  $\Gamma(\theta, t) = 2U\theta$ , and  $\mathbf{B}_i(\theta, t) = B_0$  is an equilibrium solution of the current-vortex sheet model. We consider the solution of small perturbations for the equilibrium under the linear approximation of the model.

Let us write the solution with small perturbations as

$$\Gamma(\theta, t) = 2U(\theta + \epsilon\hat{\Gamma}(\theta, t)), \quad (14a)$$

$$x(\theta, t) = \theta + \epsilon\hat{x}(\theta, t), \quad (14b)$$

$$y(\theta, t) = \epsilon\hat{y}(\theta, t), \quad (14c)$$

$$\mathbf{B}_i(\theta, t) = B_0 + \epsilon\hat{B}_i^t(\theta, t)\mathbf{t}. \quad (14d)$$

The linearized equations are obtained by expanding Eqs. (6), (7), (10), and (13), and retaining the first order terms in  $\epsilon$ ,

$$\frac{\partial\hat{\Gamma}}{\partial t}(\theta, t) = \frac{B_0}{2\rho\mu U}(\hat{B}_1^t - \hat{B}_2^t), \quad (15a)$$

$$\frac{\partial\hat{x}}{\partial t}(\theta, t) = -\frac{U}{4\pi} \int_0^{2\pi} \frac{\hat{y}(\theta, t) - \hat{y}(\theta', t)}{\sin^2[(\theta - \theta')/2]} d\theta', \quad (15b)$$

$$\frac{\partial\hat{y}}{\partial t}(\theta, t) = -\frac{U}{4\pi} \left\{ \int_0^{2\pi} \frac{\hat{x}(\theta, t) - \hat{x}(\theta', t)}{\sin^2[(\theta - \theta')/2]} d\theta' - 2 \int_0^{2\pi} \hat{\Gamma}_\theta(\theta', t) \cot\left(\frac{\theta - \theta'}{2}\right) d\theta' \right\}, \quad (15c)$$

$$\frac{\partial\hat{B}_1^t}{\partial t}(\theta, t) = -U(\hat{B}_1^t)_\theta + B_0\hat{x}_{t\theta} + B_0U(\hat{\Gamma}_{\theta\theta} - \hat{x}_{\theta\theta}), \quad (15d)$$

$$\frac{\partial\hat{B}_2^t}{\partial t}(\theta, t) = U(\hat{B}_2^t)_\theta + B_0\hat{x}_{t\theta} - B_0U(\hat{\Gamma}_{\theta\theta} - \hat{x}_{\theta\theta}). \quad (15e)$$

We express the perturbed quantities in Fourier series. The even and odd modes are coupled in the current-vortex sheet model; this differs from the linear stability analysis of the vortex sheets in the hydrodynamic flows such as inviscid vortex sheets with/without surface tension [26] and regularized vortex sheets [21,23]. The coupling of the even and odd modes in this system makes the analysis more complicated. An ansatz for the solution of this model is of the form,

$$\hat{\Gamma}(\theta, t) = P_1(t) \cos(k\theta) + Q_1(t) \sin(k\theta), \quad (16a)$$

$$\hat{x}(\theta, t) = P_2(t) \cos(k\theta) + Q_2(t) \sin(k\theta), \quad (16b)$$

$$\hat{y}(\theta, t) = P_3(t) \cos(k\theta) + Q_3(t) \sin(k\theta), \quad (16c)$$

$$\hat{B}_1^t(\theta, t) = P_4(t) \cos(k\theta) + Q_4(t) \sin(k\theta), \quad (16d)$$

$$\hat{B}_2^t(\theta, t) = P_5(t) \cos(k\theta) + Q_5(t) \sin(k\theta), \quad (16e)$$

where  $k$  is the wave number. This ansatz is substituted into Eq. (15). The integrals are calculated by applying the complex residue theorem,

$$\frac{1}{2\pi} \int_0^{2\pi} \sin(k\theta') \cot\left(\frac{\theta - \theta'}{2}\right) d\theta' = \begin{cases} -\cos(k\theta) & \text{for } k > 0, \\ 0 & \text{for } k = 0, \end{cases} \quad (17a)$$

$$\frac{1}{2\pi} \int_0^{2\pi} \cos(k\theta') \cot\left(\frac{\theta - \theta'}{2}\right) d\theta' = \begin{cases} \sin(k\theta) & \text{for } k > 0, \\ 0 & \text{for } k = 0, \end{cases} \quad (17b)$$

$$\frac{1}{4\pi} \int_0^{2\pi} \frac{\cos(k\theta) - \cos(k\theta')}{\sin^2((\theta - \theta')/2)} d\theta' = k \cos(k\theta), \quad (17c)$$

$$\frac{1}{4\pi} \int_0^{2\pi} \frac{\sin(k\theta) - \sin(k\theta')}{\sin^2((\theta - \theta')/2)} d\theta' = k \sin(k\theta). \quad (17d)$$

Thus, we have the system of equations for the amplitude  $P_i$  and  $Q_i$ , for  $1 \leq i \leq 5$ ,

$$\frac{d\mathbf{Z}}{dt} = \begin{pmatrix} A & -E \\ E & A \end{pmatrix} \mathbf{Z}, \quad (18)$$

where

$$\mathbf{Z} = (P_1 \ P_2 \ \cdots \ P_5 \ Q_1 \ Q_2 \ \cdots \ Q_5)^T, \quad (19a)$$

$$A = \begin{pmatrix} 0 & 0 & 0 & \frac{B_0}{2\rho\mu U} & -\frac{B_0}{2\rho\mu U} \\ 0 & 0 & -kU & 0 & 0 \\ kU & -kU & 0 & 0 & 0 \\ -k^2 B_0 U & k^2 B_0 U & 0 & 0 & 0 \\ k^2 B_0 U & -k^2 B_0 U & 0 & 0 & 0 \end{pmatrix}, \quad (19b)$$

$$E = \begin{pmatrix} 0 & 0 & 0 & 0 & 0 \\ 0 & 0 & 0 & 0 & 0 \\ 0 & 0 & 0 & 0 & 0 \\ 0 & 0 & k^2 B_0 U & kU & 0 \\ 0 & 0 & k^2 B_0 U & 0 & -kU \end{pmatrix}. \quad (19c)$$

The growth rates from the linearized equations are obtained by

$$\lambda(k) = 0, \quad (20a)$$

$$\lambda(k) = \pm ikU, \quad (20b)$$

$$\lambda(k) = \pm \sqrt{k^2(U^2 - v_A^2)}, \quad (20c)$$

where  $v_A = B_0/\sqrt{\rho\mu}$  denotes the Alfvén speed. The growth rate (20) indicates that the instability occurs when

$$U > v_A, \quad (21)$$

i.e., the Alfvén speed is smaller than the half of the velocity jump across the interface. This equation is expressed as  $M_A > 2$ , by defining the Alfvén Mach number  $M_A = 2U/v_A$ . The growth rate (20c) agrees with the linear stability from the MHD equations in Chandrasekhar [9] and Ren *et al.* [29]. The linear stability is identified as  $M_A \leq 2$  from Eq. (20c); however, we should be careful for  $M_A = 2$  when the growth rate (20c) becomes zero.

For further analysis, we calculate the eigenvector of the linearized equations. All eigenvalues in Eq. (20) are double roots of the characteristic equation. The eigenvalue  $\lambda = 0$  has the two independent eigenvectors,

$$\mathbf{Z}_1 = (0, 0, 0, 0, 0, 1, 1, 0, 0, 0)^T, \quad (22a)$$

$$\mathbf{Z}_2 = (1, 1, 0, 0, 0, 0, 0, 0, 0, 0)^T. \quad (22b)$$

The eigenvalues  $\lambda(k) = \pm ikU$  have four independent eigenvectors,  $\mathbf{Z}_i$ ,  $3 \leq i \leq 6$ , which are not listed here. The eigenvalues  $\lambda(k) = \pm \sqrt{k^2(U^2 - v_A^2)}$  also have the four independent eigenvectors,

$$\mathbf{Z}_i = (0, 0, 0, 0, 0, \pm v_A^2, \pm U^2, U\sqrt{\Delta}, -kU v_A \sqrt{\Delta}, kU v_A \sqrt{\Delta})^T, \quad i = 7, 8, \quad (23a)$$

$$\mathbf{Z}_i = (\pm v_A^2, \pm U^2, U\sqrt{\Delta}, -kU v_A \sqrt{\Delta}, kU v_A \sqrt{\Delta}, 0, 0, 0, 0, 0)^T, \quad i = 9, 10, \quad (23b)$$

by defining  $\Delta = U^2 - v_A^2$ . Thus, the linear system has a full set of eigenvectors when  $\Delta \neq 0$ . However, when  $\Delta$  vanishes,

the eigenvalues  $\lambda(k) = \pm \sqrt{k^2(U^2 - v_A^2)}$  become zero, and the number of eigenvectors associated with them reduces to 2, which yields the solution of the form proportional to  $t$ . This resonance behavior indicates that the interface is unstable for the limiting value of the Alfvén Mach number,  $M_A = 2$ . Therefore, the criterion for the linear stability of the MHD KHI is concluded as  $M_A < 2$ . The resonance behavior in the limiting value is highly contrasted to the KHI in the pure hydrodynamic flows.

#### IV. NUMERICAL RESULTS

In this section, we present numerical results from the current-vortex sheet model. The physical variables are nondimensionalized to  $\mathbf{x}/L \rightarrow \mathbf{x}$ ,  $\gamma/(2U) \rightarrow \gamma$ ,  $2Ut/L \rightarrow t$ , and  $\mathbf{B}_i/B_0 \rightarrow \mathbf{B}_i$ , where  $\mathbf{B}(t=0) = B_0 \mathbf{t}$ . The equation for the vortex sheet strength (11) is nondimensionalized to

$$\frac{d\gamma}{dt} = \frac{1}{M_A^2 s_\theta} (\mathbf{B} \cdot \mathbf{j}_s)_\theta, \quad (24)$$

which introduces the Alfvén Mach number. Equation (13) remains the same after nondimensionalization.

##### A. Numerical method

It is well known that the Kelvin-Helmholtz instability develops a roll-up due to the formation of a singularity [30], and this produces a difficulty in numerical computations [1]. To overcome it, we apply the vortex blob method, which gives a desingularization parameter  $\delta > 0$  to the integral kernel of the Birkhoff-Rott equation, following Krasny [21]. The regularized Birkhoff-Rott equation, after nondimensionalization, is given by

$$u(\theta, t) = \frac{1}{2} \int_0^1 \frac{\sinh 2\pi(y - y')}{\cosh 2\pi(y - y') - \cos 2\pi(x - x') + \delta^2} \times \gamma(\theta', t) s_\theta(\theta') d\theta', \quad (25a)$$

$$v(\theta, t) = -\frac{1}{2} \int_0^1 \frac{\sin 2\pi(x - x')}{\cosh 2\pi(y - y') - \cos 2\pi(x - x') + \delta^2} \times \gamma(\theta', t) s_\theta(\theta') d\theta', \quad (25b)$$

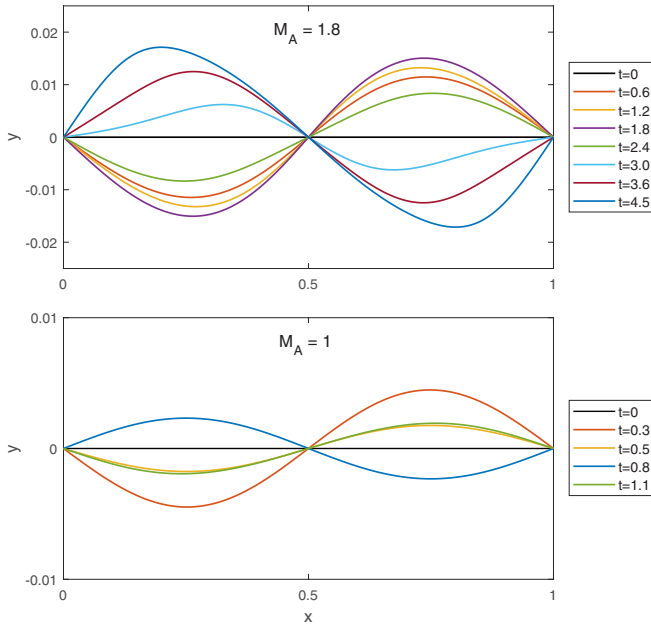


FIG. 1. Evolution of the vortex sheet for  $M_A = 1.8$  and 1.0.

denoting  $x = x(\theta, t)$ ,  $y = y(\theta, t)$ , and  $x' = x(\theta', t)$ ,  $y' = y(\theta', t)$ . The  $\delta$  parameter in Eq. (25) acts as the numerical viscosity on the interface. A small value of the regularization parameter provides fine resolution of the interface, but it requires a large number of points and makes the computation expensive [21,22]. Thus, we choose  $\delta = 0.15$  for all the results in this section. This value of  $\delta$  was used in the previous works on the vortex sheet in the MHD flows [18–20].

To solve the equations numerically, we discretize the interface  $\{\mathbf{x}_j\}_{j=0}^N$ , the vortex sheet strength  $\{\gamma_j\}_{j=0}^N$ , and the magnetic fields  $\{\mathbf{B}_{ij}\}_{j=0}^N$ ,  $i = 1, 2$ . The trapezoidal rule is applied to evaluate the interface velocity (25). For time-advancing of Eqs. (6), (11), and (13), the standard fourth-order Runge-Kutta method is employed. All the spatial derivatives are calculated by the central difference, except the case of  $M_A \approx 2$  which will be explained below.

The initial condition is set to

$$x(\theta, 0) = \theta, \quad y(\theta, 0) = 0, \quad \Gamma(\theta, 0) = \theta - a_0 \sin(2\pi\theta), \quad (26a)$$

$$\mathbf{B}_i(\theta, 0) = \mathbf{e}_x, \quad \text{for } i = 1, 2, \quad (26b)$$

and  $0 \leq \theta \leq 1$ , by giving a perturbation only to the circulation of the interface, where  $\mathbf{e}_x$  is the unit vector in the  $x$  axis. The initial amplitude is set to  $a_0 = 0.01$ . This initial condition was used in Baker and Nachbin [26]. To present numerical results, we divide the regime into  $M_A > 2$  and  $M_A < 2$ , from the linear stability analysis.

### B. Results for $M_A < 2$

We first consider the regime of  $M_A < 2$  for simulations and choose  $M_A = 1.8$  and 1.0 as representative cases of stability. For both cases, the number of points and time step are given by  $N = 200$  and  $\Delta t = 5 \times 10^{-4}$ .

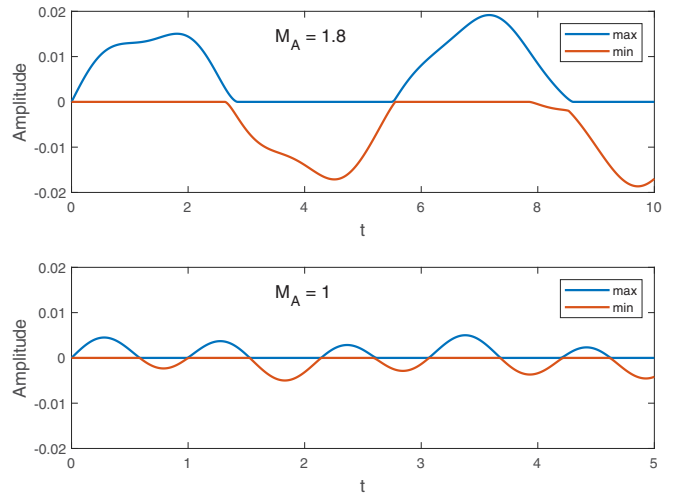


FIG. 2. Amplitude of the vortex sheet for  $M_A = 1.8$  and 1.0. The blue (upper) curve represents the maximum height of the sheet, and the red (lower) curve represents the minimum depth of the sheet.

Figure 1 shows the evolution of the vortex sheet for  $M_A = 1.8$  and 1.0. The scale of the  $y$  axis is enlarged for a clear view. For both cases, the vortex sheet oscillates longitudinally and roll-up is not formed, indicating the stability of the sheet. However, the sheet for  $M_A = 1.8$  has a much larger amplitude and oscillates more dynamically than that for  $M_A = 1.0$ . Let us look closer into the evolution of the sheet for  $M_A = 1.8$ . The sheet grows fast initially and slows down at  $0.6 < t < 1.8$ . The sheet for  $0.5 < \theta < 1$  then goes down until  $t = 4.5$ . We see that the peak of the sheet moves largely in the horizontal direction. This transverse oscillation will be due to the occurrence of the Alfvén surface wave, which propagates on the interface. For the case of  $M_A = 1.0$ , the sheet moves transversely only a little. The Alfvén surface wave is important in space plasma and its behavior was investigated by many authors [27,28].

The amplitude of the vortex sheet for  $M_A = 1.8$  and 1.0 is plotted in Fig. 2. The blue (upper) curve represents the maximum height of the sheet, and the red (lower) curve represents the minimum depth of the sheet. The amplitude of the sheet for  $M_A = 1.8$  goes up and down irregularly from the Alfvén oscillation, while that for  $M_A = 1.0$  oscillates relatively regularly. The oscillation period of the sheet of  $M_A = 1.8$  is about five times longer than that of  $M_A = 1.0$ . From Eq. (20), the linear stability analysis predicts the period of oscillation  $T = 1/(0.5 + \sqrt{1^2 - 0.5^2}) = 0.73$  for  $M_A = 1.0$ , which is slightly shorter than the numerical result in Fig. 2.

To examine the oscillatory behavior of the vortex sheet, we plot the magnetic field  $B_i^t$  and current sheet strength  $j_s$  for the case of  $M_A = 1.8$ . Figure 3 shows that the current sheet strength of the peak and valley of the sheet is strong when the sheet approaches the maximum and minimum. We also observe that the current sheet strength of the peak and valley is fairly strong at  $t = 3.2$ , where the peak and valley begin to shift transversely in the opposite direction. The color pattern of the magnetic field is similar to the current sheet strength, although their values are quantitatively different.

In addition, we run simulations for  $M_A$  close to 2 and have difficulties in the computation. For  $M_A \approx 2$ , the computation

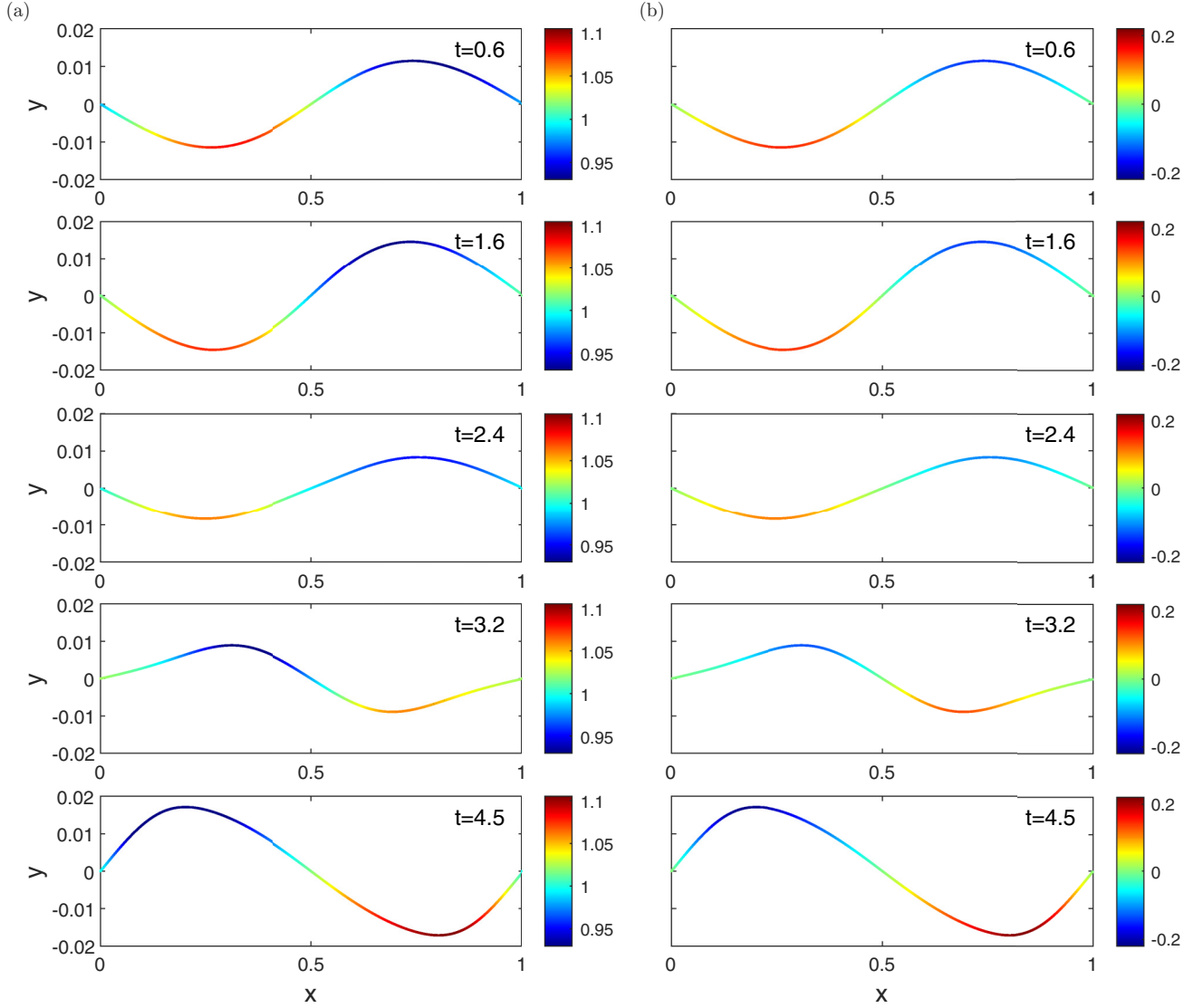


FIG. 3. Magnetic field and current sheet strength for  $M_A = 1.8$ . (a) Magnetic field  $B_1'$ , and (b) current sheet strength  $j_s$ .

often stops in the middle of run. In this case, the surface wave is stronger and this may influence the numerical stability. We pay attention to the first and second terms in Eq. (13), which can be regarded as a type of the advection equation where  $\gamma$  plays as the wave speed. Therefore, to circumvent the numerical instability, we change the central difference for  $\gamma(B_i')_\theta$  in Eq. (13) into the second-order upwind difference:

$$\gamma \frac{\partial B_1'}{\partial \theta} \approx \begin{cases} \gamma_j \frac{3B_{1,j}' - 4B_{1,j-1}' + B_{1,j-2}'}{2\Delta\theta} & \text{for } \gamma_j \geq 0, \\ \gamma_j \frac{-B_{1,j+2}' + 4B_{1,j+1}' - 3B_{1,j}'}{2\Delta\theta} & \text{for } \gamma_j < 0. \end{cases} \quad (27)$$

The forward and backward differences in Eq. (27) are switched for  $\gamma(B_2')_\theta$ , because of the difference sign of  $\gamma(B_2')_\theta$  in Eq. (13).

The evolution of the vortex sheet for  $M_A = 1.9$  by employing the upwind scheme is shown in Figs. 4 and 5. The numerical parameters are given by  $N = 400$  and  $\Delta t = 10^{-4}$ . In Fig. 4, the profiles at  $t = 1$  and 2 are similar to the case of  $M_A = 1.8$ . However, the sheet at the center begins to steepen

at  $t = 2.7$ , and a kink appears at  $t = 3.0$ . Subsequently, roll-up is evolved at the center of the sheet, as shown in Fig. 5. The  $x$  and  $y$  axis are of the same scale in Fig. 5, while they

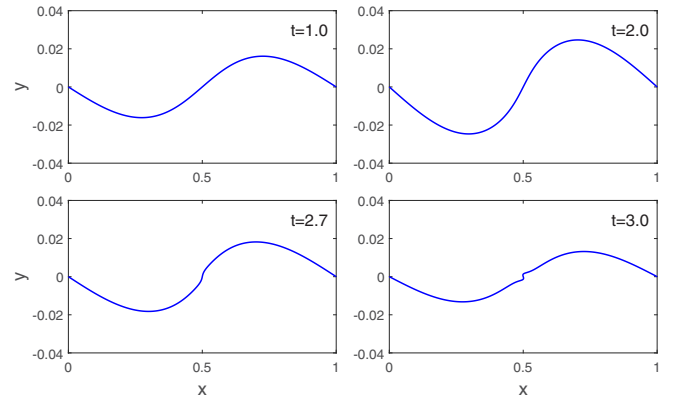


FIG. 4. Evolution of the vortex sheet for  $M_A = 1.9$  at early times.

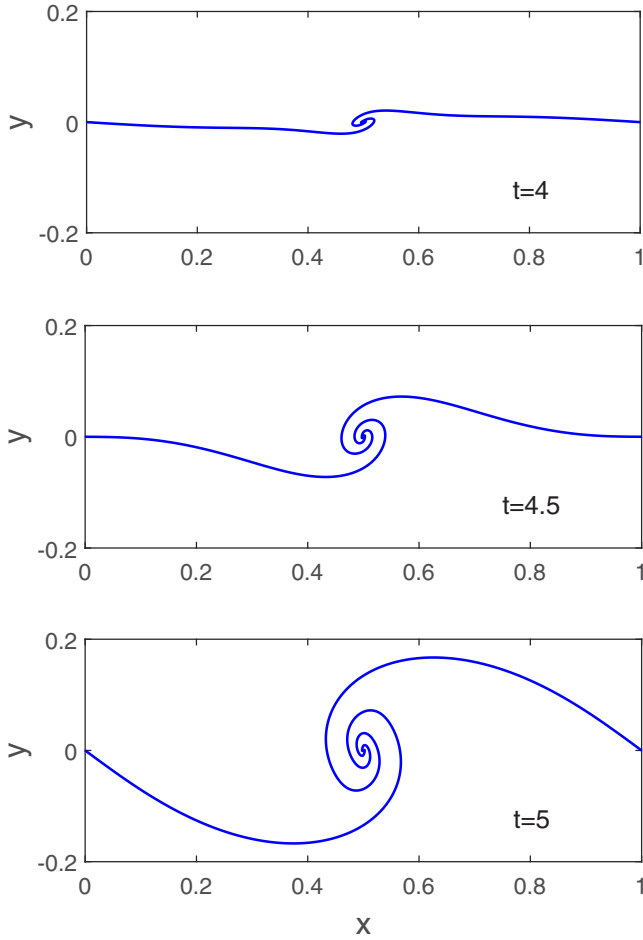


FIG. 5. Evolution of the vortex sheet for  $M_A = 1.9$  at  $t \geq 4$ . The  $x$  and  $y$  axis are of the same scale.

are different in Fig. 4. We also observe corrugations on the sheet at  $t = 4$  and  $4.5$ . The magnetic field  $B'_1$  and vortex sheet strength  $\gamma$  on the sheet for  $M_A = 1.9$ , at  $t = 2, 2.7, 3$  and  $4$ , are plotted in Fig. 6. Both  $B'_1$  and  $\gamma$  are disturbed at  $t = 2.7$  and have a peak at the center at  $t = 3$ , which will be excited

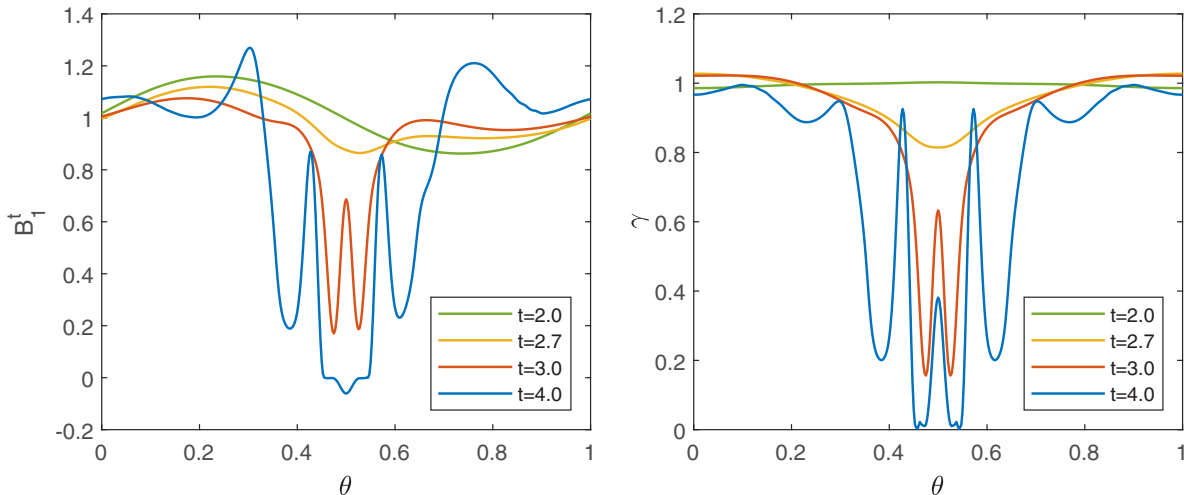


FIG. 6. Magnetic field  $B'_1$  and vortex sheet strength on the sheet for  $M_A = 1.9$ .

by the singularity formation. We see that the wave propagates outward at  $t = 4$ .

We also attempted to calculate the critical Alfvén Mach number,  $M_A = 2$ . The sheet for  $M_A = 2$  is unstable and roll-up is evolved, similarly as  $M_A = 1.9$ . (The result is not shown here.) The instability in the limit of  $M_A \rightarrow 2$  is consistent with our linear stability analysis, and this instability would be expected, because resonance of eigenvalues may occur when  $M_A$  is close to 2.

The instability for  $M_A \approx 2$  can be further explained by nonlinear surface waves. Hunter and Thoo [12] propose an asymptotic equation for nonlinear surface waves on the KHI in an incompressible MHD flow and show that an initially linearly stable solution, under a certain condition, develops a singularity in finite time, resulting in the instability of the solution. (See also Ali and Hunter [31].) They discuss that surface waves propagate with distinct speeds  $\lambda_i = U \pm \sqrt{-\Delta}$ ,  $i = 1, 2$ , and as  $\Delta$  decreases to zero, the wave speeds  $\lambda_1$  and  $\lambda_2$  coalesce and give rise to instability. Here,  $\Delta$  is the same as that defined in Sec. 3, in our setting. Therefore, their argument is in accordance with our linear stability analysis. Our numerical results indicate that the nonlinear instability for  $M_A \approx 2$  is closely related with the propagation of surface waves.

### C. Results for $M_A > 2$

For simulations of the unstable regime, we choose  $M_A = \infty, 10, 5$ , and  $3$  as representative cases. The number of points and time step are given by  $N = 1600$  and  $\Delta t = 5 \times 10^{-5}$  for  $M_A = 10$ , and  $N = 800$  and  $\Delta t = 10^{-4}$  for  $M_A = 5$  and  $3$ . For  $M_A = \infty$ , the numerical parameters are given by  $N = 1600$  and  $\Delta t = 0.005$ , since there is no magnetic field applied to the flow.

Figure 7 shows the evolution of the vortex sheet for  $M_A = \infty$  and  $M_A = 10$ . In both cases, the spiral cores roll up strongly and the outer spiral turns stretch at late times. We observe that the outer spiral turns of  $M_A = 10$  stretch further out than those of  $M_A = \infty$  at  $t = 4$ , and the maximum  $y$  value of  $M_A = 10$  is slightly lower. Figure 8 shows the evolution of

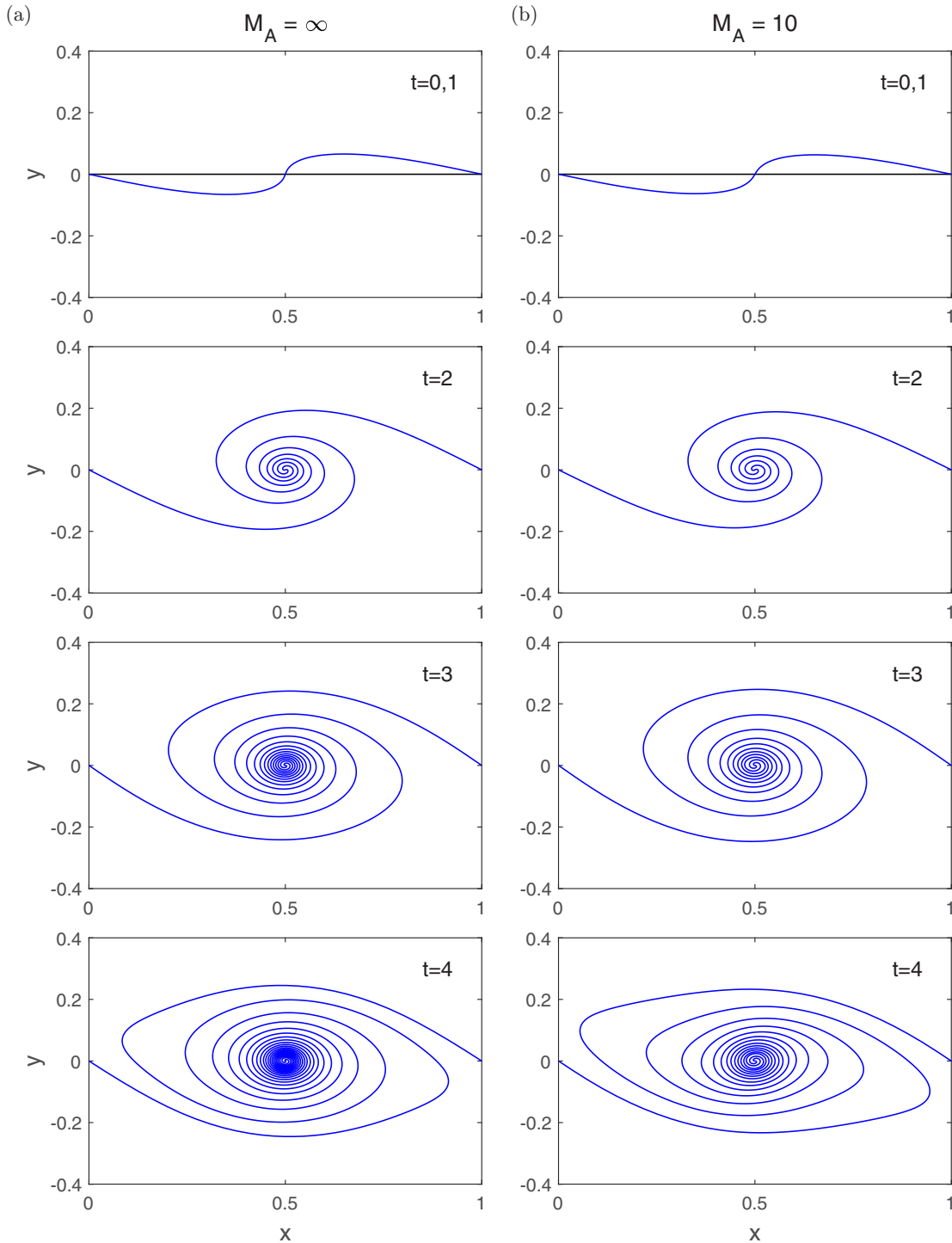


FIG. 7. Evolution of the vortex sheet for (a)  $M_A = \infty$  and (b)  $M_A = 10$ .

the vortex sheet for  $M_A = 5$  and  $3$ . For  $M_A = 5$ , the roll-up of the spiral core is weakened significantly and the spiral is pinched and stretched at late times. For  $M_A = 3$ , the sheet has only a few spiral turns and, the width of the sheet is more narrowed at late times. The results in Fig. 8 demonstrates acting of an induced force to push in longitudinally and stretch out transversely as the magnetic field increases.

Figure 9 plots the magnetic field  $B_1^t$  and current sheet strength  $j_s (= B_1^t - B_2^t)$  along the sheet for  $M_A = 10$  and  $3$ .

The magnetic field  $B_1^t$  is large at the center of the sheet at early times and increases drastically at  $\theta = 0$  and  $1$  (corresponding to the starting point of the sheet) at late times for both cases of  $M_A = 10$  and  $3$ . At  $t = 4$ , the magnetic field at  $\theta = 0$  reaches  $49.2$  for  $M_A = 10$  and  $17.1$  for  $M_A = 3$ , which are not shown here. There are significant differences in the magnetic field at  $t = 4$  between  $M_A = 10$  and  $3$ . For  $M_A = 10$ , the peaks increases rather gradually from the center to the outside, and the differences of  $B_1^t$  at  $\theta = 0$  from other points in the sheet

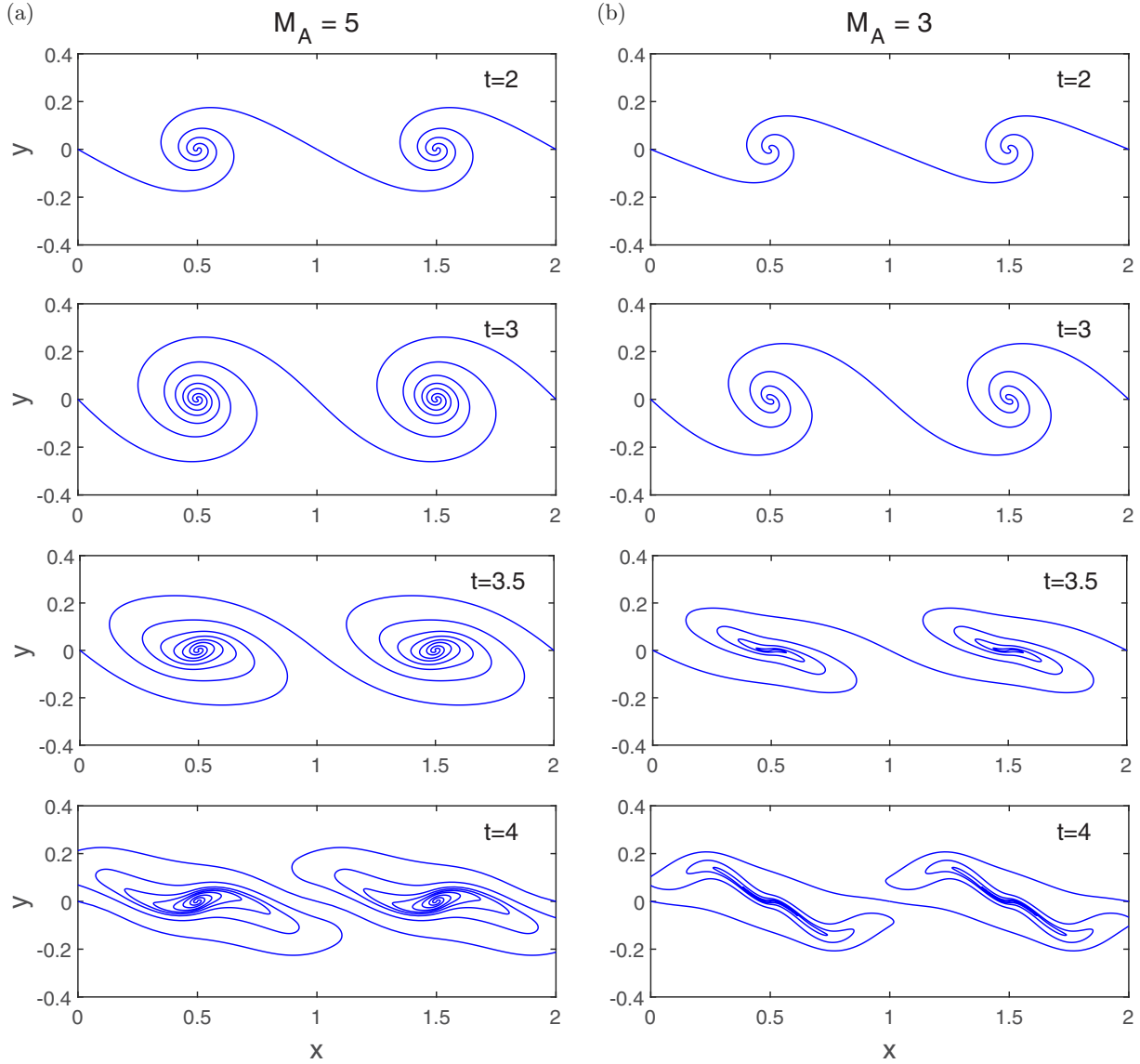


FIG. 8. Evolution of the vortex sheet for (a)  $M_A = 5$  and (b)  $M_A = 3$ .

are very large, whereas for  $M_A = 3$ , several large peaks form over the sheet irregularly and their intensities are comparable. The current sheet strength for  $M_A = 10$  is the largest at about  $\theta = 0.4$  at  $t = 1$ , and the peak is shifted to  $\theta = 0.08$  at  $t = 4$ . In the case of  $M_A = 3$ , the peak of the current sheet strength also shifts to the outside up to  $t = 3$ , and the peaks of different signs are formed at  $t = 4$ . Note that  $B_2^t$  is not drawn here, because of the symmetric relation between  $B_1^t$  and  $B_2^t$ , i.e.,  $B_2^t(\theta) = B_1^t(1 - \theta)$ . We plot the temporal growth of the maximum of the magnetic field  $B_1^t$  for  $M_A = 10, 5$ , and  $3$  in Fig. 10. It shows that the peak of  $B_1^t$  grows faster for larger  $M_A$ , or smaller initial magnetic field.

The vortex sheet strengths along the sheet for  $M_A = \infty, 10$ , and  $3$  are plotted in Fig. 11. The vortex sheet strengths for  $M_A = \infty$  and  $10$  are concentrated on the center of the sheet, and the peak of the vortex sheet strength for  $M_A = 10$  is slightly lower than that for  $M_A = \infty$ . For the case of  $M_A = 3$ , the vortex sheet strength is the strongest at the center up to  $t = 2$ . At  $t = 4$ , the sheet strength has large oscillations with

a complex structure. The peak at the center is much decreased, unlike other cases, and the maximum is at the outside, not at the center.

Figure 12 shows the magnetic field  $B_1^t$  and current sheet strength  $j_s$  along the sheet for  $M_A = 10$  and  $M_A = 3$ , at  $t = 4$ . This figure confirms the result of Fig. 9 and provides a clearer view of the magnetic field and current sheet strength. In Fig. 12, the magnetic field  $B_1^t$  for  $M_A = 10$  is the strongest at the outer arm of the spiral and is weak in the inner spiral turns. For  $M_A = 3$ , the magnetic field is also the strongest around the starting and ending points of the sheet and is relatively strong in some parts of the inner turns. The current sheet strength for  $M_A = 10$  is weak at the outmost spiral turn, in contrast to the magnetic field, and is the strongest at the second outer spiral turn, while the corresponding lower turn of the double spiral is the strongest in negative. The sign of the current sheet strength in each spiral turn from outside to inside alternates and its intensity decreases. For  $M_A = 3$ , the current sheet strength in the upper (lower) second outer turn of the spiral is the

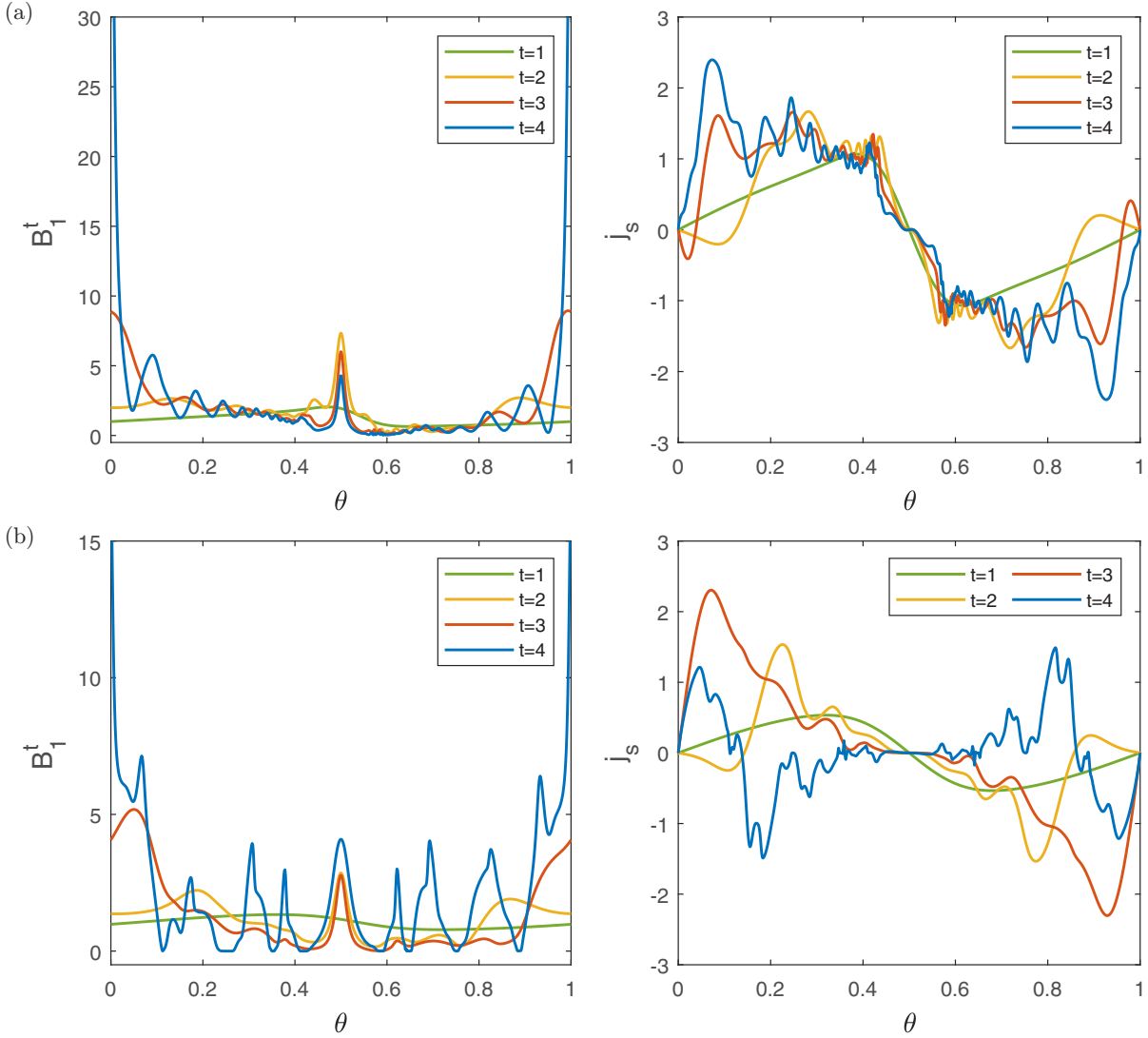


FIG. 9. Magnetic field  $B_1^t$  and current strength  $j_s (= B_1^t - B_2^t)$  along the sheet. (a)  $M_A = 10$  and (b)  $M_A = 3$ .

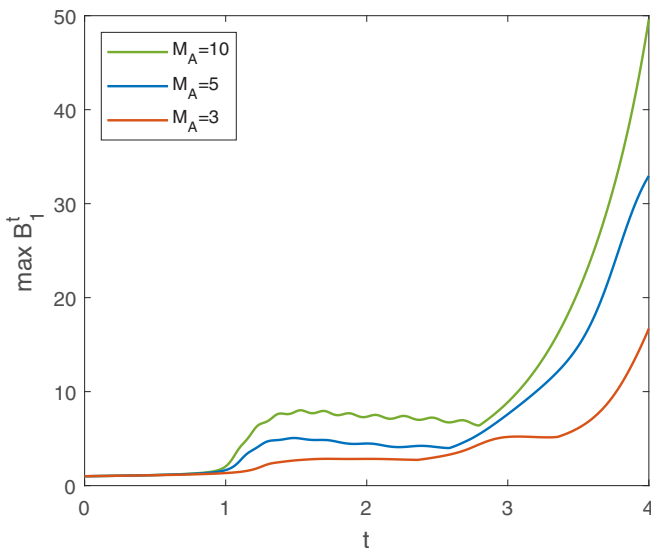


FIG. 10. Growth of the maximum of  $B_1^t$  for  $M_A = 10, 5,$  and  $3$ .

strongest in negative (positive) and is weak in the inner turns. The peak of  $j_s$  in Fig. 9(a) corresponds to the upper second outer spiral turn in Fig. 12(a), and the valley of  $j_s$  near  $\theta = 0.2$  in Fig. 7(b) corresponds to the upper second outer spiral turn in Fig. 12(b).

Figure 13 plots the vortex sheet strength for  $M_A = 10$  and  $M_A = 3$ , at  $t = 4$ . For  $M_A = 10$ , the sheet strength is concentrated on the innermost core of the spiral, which is barely observable, and is positive over the sheet, whereas for  $M_A = 3$ , the sheet strength is the strongest in the outer arm of the sheet and oscillates in sign over the sheet.

### V. CONCLUSIONS

We have studied the stability and evolution of the KHI in a MHD flow by describing the interface by a current-vortex sheet. We examine the linear stability of the current-vortex sheet model and obtain the growth rate of the interface. We show that the interface is linearly stable for  $M_A < 2$  where the magnetic field is larger than the half of the velocity jump,

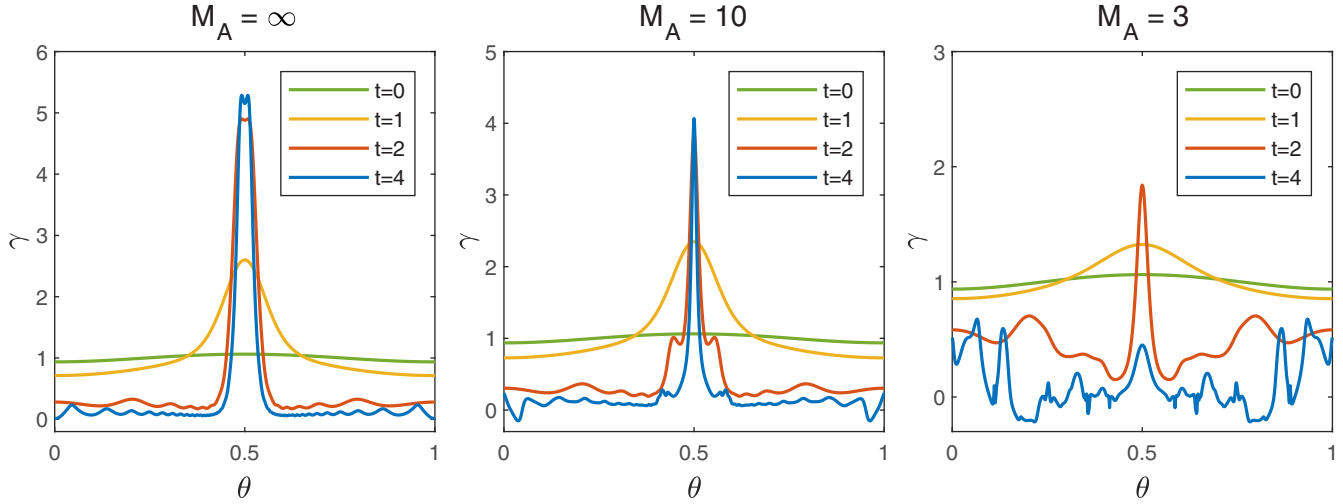


FIG. 11. Vortex sheet strength along the sheet for  $M_A = \infty, 10,$  and  $3.$

setting  $\rho\mu = 1.$  Furthermore, it is revealed that the interface is linearly unstable in the limit of the critical Alfvén Mach number  $M_A = 2,$  because of resonance of eigenvalues.

We consider a parallel magnetic field to the interface initially. The normal component of the magnetic field is zero at  $t = 0$  and remains unchanged at  $t > 0.$  One may generalize the model to include the normal component of the magnetic field. The evolution equation for the normal component of the magnetic field can be derived easily. We have checked that even with the normal component of the magnetic field, the growth rate of the linear stability of the KHI remains the same.

We have conducted the numerical simulations for the current-vortex sheet for both regimes of  $M_A < 2$  and  $M_A > 2.$

The numerical results show the stabilizing effects of the magnetic field on the evolution of the current-vortex sheet when the magnetic field is sufficiently large. For the regime  $M_A < 2,$  the sheet oscillates both longitudinally and transversely, in general. The transverse surface wave is pronounced for a large  $M_A,$  or small magnetic field. Remarkably, the interface is nonlinearly unstable for  $M_A$  close to  $2,$  for  $M_A < 2,$  which may be due to the propagation of surface waves.

For the regime  $M_A > 2,$  the roll-up of the spiral is weakened and the spiral is more pinched and stretched for smaller  $M_A.$  There are significant differences of the evolution between large and small values of  $M_A.$  For a large  $M_A,$  the magnetic field is strong only at the outer spiral turn, but for a small  $M_A,$

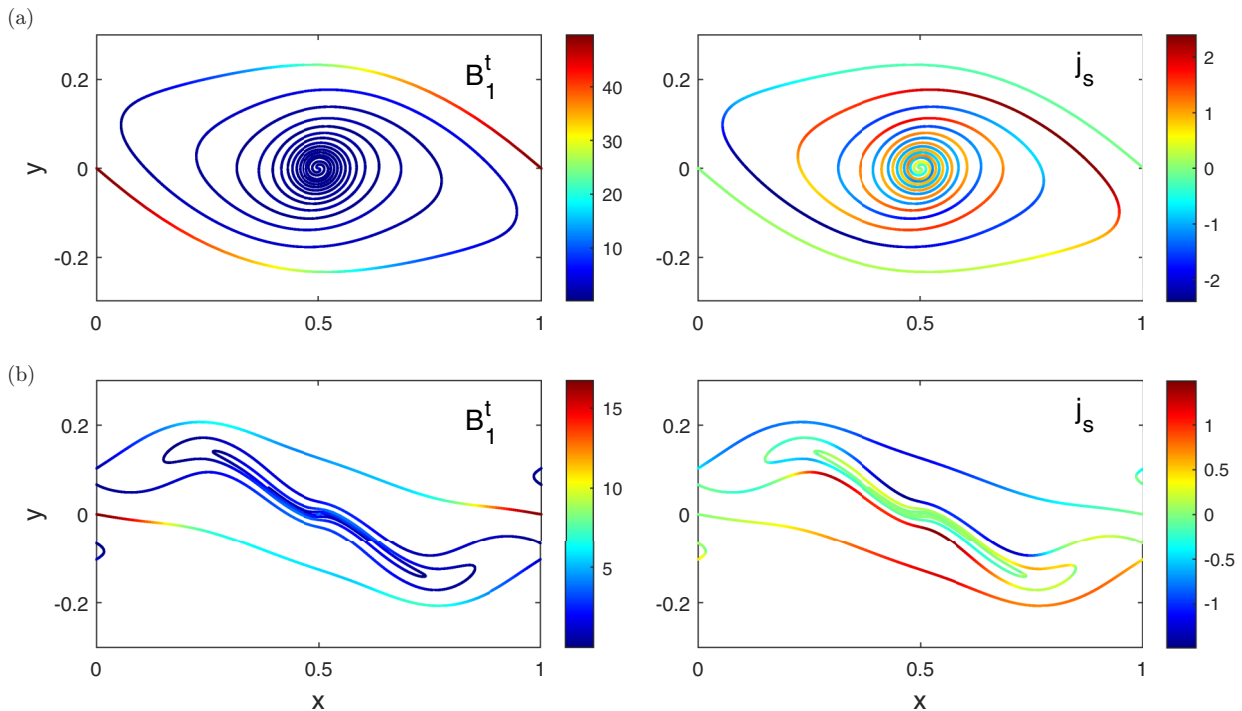


FIG. 12. Magnetic field  $B_1^t$  and current sheet strength  $j_s$  at  $t = 4.$  (a)  $M_A = 10$  and (b)  $M_A = 3.$

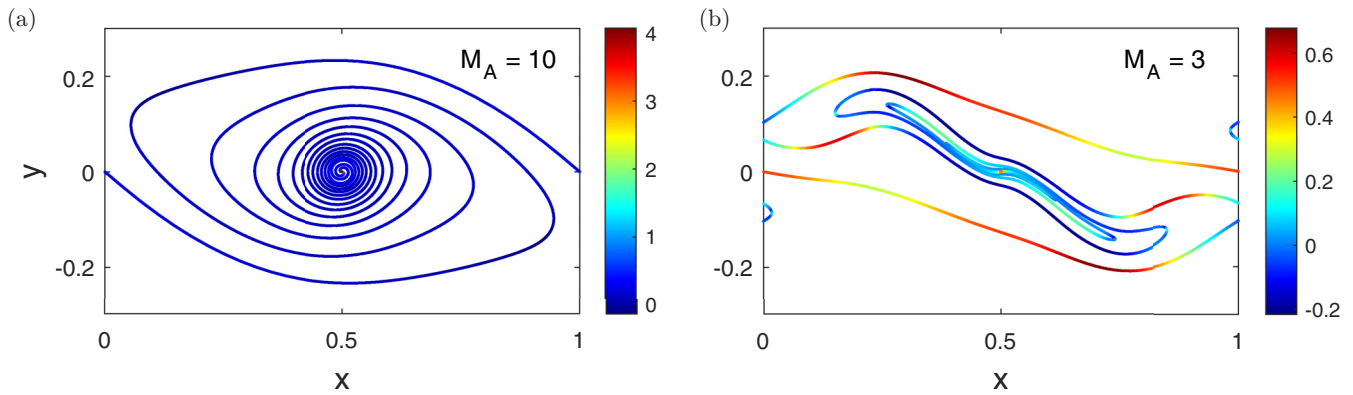


FIG. 13. Vortex sheet strength at  $t = 4$ . (a)  $M_A = 10$  and (b)  $M_A = 3$ .

it is relatively strong also in the inner spiral turns. For a large  $M_A$ , the vortex sheet strength is the strongest at the center, whereas for a small  $M_A$ , the peak at the center is decreased and the sheet strength at the outer turn becomes large at late times.

The nonlinear instability for  $M_A \approx 2$  is of special interest. It seems that the sheet tends to steepen, due to surface waves, and forms a singularity. More theoretical and numerical investigations on the formation of the singularity and the effect of surface waves in this regime are called for. The numerical investigation for the singularity formation near the critical time requires the computation of the vortex method with zero regularization parameter [32,33], which is a sophisticated task.

The vortex sheet model is a sharp interface model in an incompressible and ideal fluid. This model provides useful virtues and insights in the understanding of the dynamics of the KHI, in general. However, there are limitations of the model in the application of real astrophysical system, particularly with finite thickness [7]. The vortex sheet model is not suitable to describe the astrophysical phenomena such as the tearing instability which leads to form “magnetic

islands” [15], and the coalescence instability in which parts of the current sheet merge or separate [34]. The extension of the vortex sheet model, or other vortex models, to deal with these phenomena is an interesting subject to challenge.

One may further consider the formation of turbulence from the vortex sheet model. Tryggvason *et al.* [35] showed that the limiting solution of the vortex blob model reproduced many features associated with viscous flows with increasing Reynolds number. Numerical simulations of the KHI by using the vortex blob model showed the appearance of chaotic and turbulent motions of the interface at the late nonlinear stage [22,23,36]. The long-time computation of the magnetic KHI by using the vortex sheet model requires sophisticated numerical procedures. We leave this subject for future study.

#### ACKNOWLEDGMENTS

The authors thank the anonymous referees for their valuable comments, which improved the paper. This work was supported by the National Research Foundation of Korea (NRF) grant funded by the Korea government (MSIT) under Grant No. RS-2023-00242094.

- 
- [1] G. Birkhoff, *Proceedings of Symposia in Applied Mathematics* (American Mathematical Society, Providence, RI, 1962), Vol. XIII, p. 55.
  - [2] S. A. Thorpe, *J. Fluid Mech.* **708**, 1 (2012).
  - [3] A. Briard, B.-J. Grea, and F. Nguyen, *Phys. Rev. E* **106**, 065201 (2022).
  - [4] W. D. Smyth and J. N. Moum, *Oceanography* **25**, 140 (2012).
  - [5] M. Birkinshaw, *Astrophys. Space Sci.* **242**, 17 (1997).
  - [6] H. Hasegawa *et al.*, *Nature (London)* **430**, 755 (2004).
  - [7] M. Faganello and F. Califano, *J. Plasma Phys.* **83**, 535830601 (2017).
  - [8] V. N. Gamezo, A. M. Khokhlov, E. S. Oran *et al.*, *Science* **299**, 77 (2003).
  - [9] S. Chandrasekhar, *Hydrodynamic and Hydromagnetic Stability* (Oxford University Press, Oxford, UK, 1961).
  - [10] A. Miura and P. L. Pritchett, *J. Geophys. Res.* **87**, 7431 (1982).
  - [11] K. I. Ilin, Y. L. Trakhinin, and V. A. Vladimirov, *Phys. Plasmas* **10**, 2649 (2003).
  - [12] J. K. Hunter and J. B. Thoo, *J. Hyper. Differ. Equat.* **08**, 691 (2011).
  - [13] A. Malagoli, G. Bodo, and R. Rosner, *Astrophys. J.* **456**, 708 (1996).
  - [14] R. B. Dahlburg, P. Boncinelli, and G. Einaudi, *Phys. Plasmas* **4**, 1213 (1997).
  - [15] R. Keppens, G. Toth, R. H. J. Westermann, and J. P. Goedbloed, *J. Plasma Phys.* **61**, 1 (1999).
  - [16] S. H. Lai and L. H. Lyu, *J. Geophys. Res.* **111**, A01202 (2006).
  - [17] Y. Liu, Z. H. Chen, H. H. Zhang, and Z. Y. Lin, *Phys. Fluids* **30**, 044102 (2018).
  - [18] C. Matsuoka, K. Nishihara, and T. Sano, *Fluid Dyn. Res.* **46**, 031416 (2014).
  - [19] C. Matsuoka, K. Nishihara, and T. Sano, *J. Nonlin. Sci.* **27**, 531 (2017).
  - [20] C. Matsuoka, K. Nishihara, and T. Sano, *High Energy Density Phys.* **31**, 19 (2019).
  - [21] R. Krasny, *J. Comput. Phys.* **65**, 292 (1986).

- [22] S.-I. Sohn, D. Yoon, and W. Hwang, *Phys. Rev. E* **82**, 046711 (2010).
- [23] S.-I. Sohn, *Phys. Fluids* **26**, 044105 (2014).
- [24] T. Y. Hou, J. S. Lowengrub, and M. J. Shelley, *Phys. Fluids* **9**, 1933 (1997).
- [25] S.-I. Sohn and W. Hwang, *J. Phys. Soc. Jpn.* **74**, 1472 (2005).
- [26] G. Baker and A. Nachbin, *SIAM J. Sci. Comput.* **19**, 1737 (1998).
- [27] R. Gerwin, *Phys. Fluids* **10**, 2164 (1967).
- [28] L. Chen and A. Hasegawa, *J. Geophys. Res.* **79**, 1024 (1974).
- [29] H. Ren *et al.*, *Phys. Plasmas* **18**, 022110 (2011).
- [30] D. W. Moore, *Proc. R. Soc. London A* **365**, 105 (1979).
- [31] G. Ali and J. K. Hunter, *Q. Appl. Math.* **61**, 451 (2003).
- [32] R. Krasny, *J. Fluid Mech.* **167**, 65 (1986).
- [33] S.-I. Sohn, *Phys. Fluids* **25**, 014106 (2013).
- [34] J. Mahapatra, A. Bokshi, R. Ganesh, and A. Sen, *Phys. Plasmas* **28**, 072103 (2021).
- [35] G. Tryggvason, W. J. A. Dahm, and D. Sbeih, *ASME Trans. J. Fluids Eng.* **113**, 31 (1991).
- [36] S.-C. Kim, J.-Y. Lee, and S.-I. Sohn, *J. Phys. Soc. Jpn.* **72**, 1968 (2003).